Supplementary Materials

Dynamical Characterization

The dynamical characteristics of the flow-fields around the flapping foil at different parametric values are demonstrated in the main article using the phase-averaged vorticity contour plots. As quantitative proof, the average correlation of the vorticity fields at different flapping cycles are also presented there. The $C_L - C_D$ phase portraits and the morlet wavelet transforms (Grossmann *et al.* 1990) of the C_D time histories of the corresponding parametric cases are presented here as supplementary material. A closed loop orbit in the phase diagram indicates periodic dynamics. On the other hand, during quasi-periodicity, the trajectory neither repeats exactly nor deviates significantly but returns to the neighbourhood of its previous positions and fills the phase space as a toroid. In the chaotic state, the long term behaviour of the trajectory becomes unpredictable, though it remains bounded within a chaotic attractor visible in the phase plot. Morlet wavelet transforms are used for visualizing the time-frequency behaviour of a signal (Grossmann *et al.* 1990). These are presented in terms of scalogram plots where the x and y-axes represent the time and equivalent frequencies, respectively. An organized narrow frequency band in the wavelet plot corresponds to periodic dynamics, whereas the presence of a modulating frequency band along with incommensurate frequency bands are indicative of a quasi-periodic state. A broad-banded frequency spectra in the wavelet plot is resulted by the chaotic dynamics.

In this supplementary document, figures 1 and 2 presents the $C_L - C_D$ plots for the parametric cases presented in figures 9 and 10 of the main article, respectively. The wavelet transform plots of the respective cases are shown in figures 3 and 4 of this supplementary document. Variation in the dynamical states of the aerodynamic loads for different pitching amplitudes is shown in figures 5 and 6. Similarly, the influence of different pitching-axis locations is demonstrated in figures 7 and 8. Figures 9 and 10 present the dynamical states at different flapping frequencies. The effect of varying the foil thickness is demonstrated in figures 11 and 12. Finally, the $C_L - C_D$ plots and the wavelet spectra for different kinematic patterns are shown in figures 13 and 14. Clearly, the dynamical signatures reflected through the aerodynamic loads as presented in this document match perfectly with the reportings of the main article.

REFERENCES

Grossmann, A, Kronland-Martinet, Richard & Morlet, J 1990 Reading and understanding continuous wavelet transforms. In *Wavelets*, pp. 2–20. Springer.

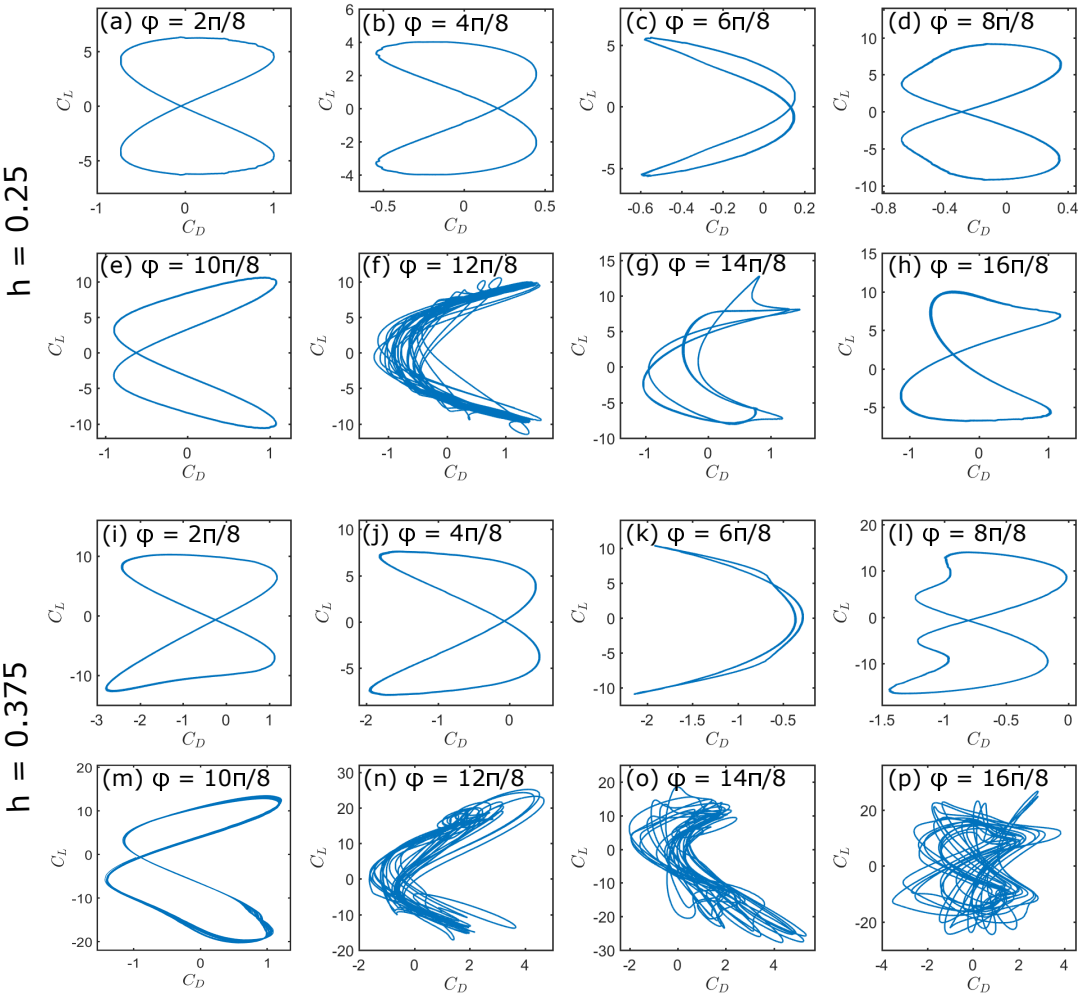

FIGURE 1. $C_L - C_D$ phase portraits at different ϕ values; $(a - h)$ at $h = 0.25$ and $(i - p)$ at $h = 0.375$.

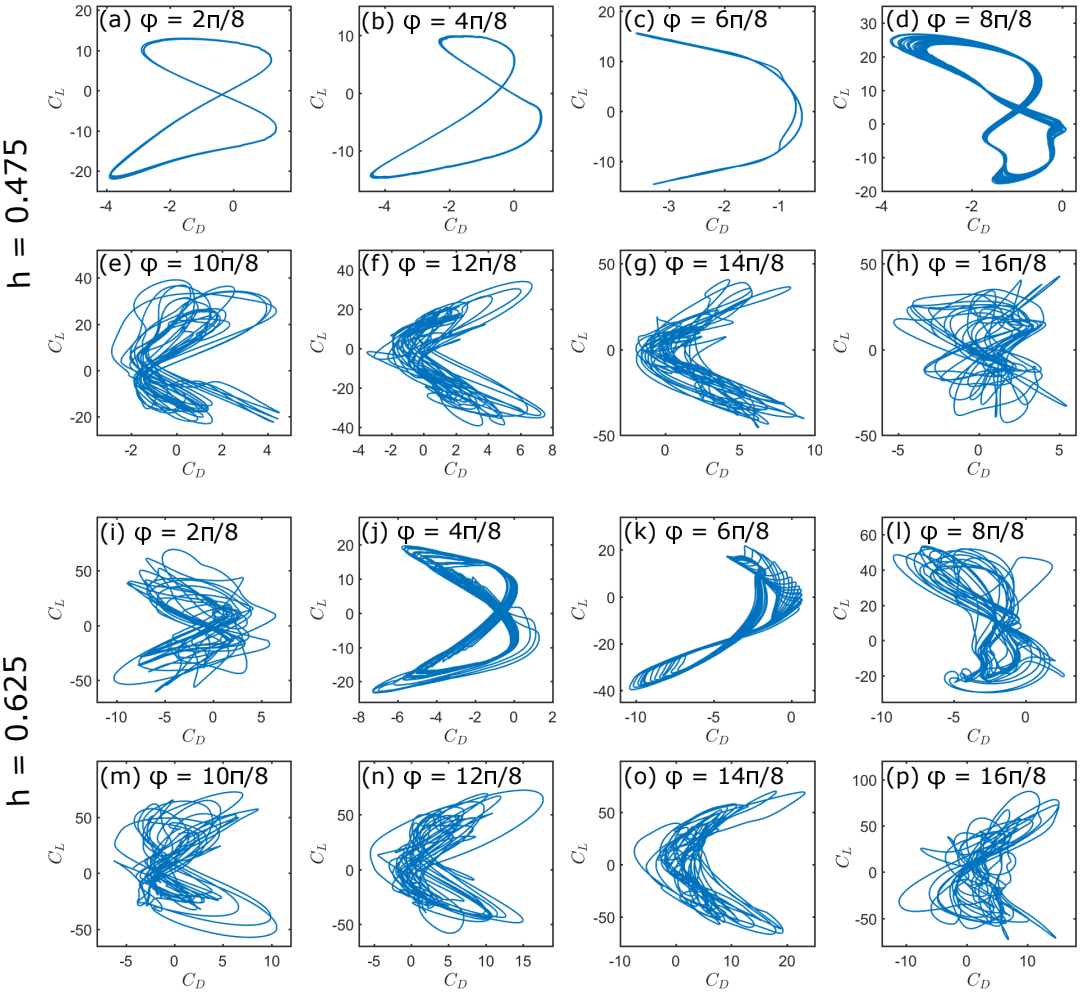

FIGURE 2. $C_L - C_D$ phase portraits at different ϕ values; $(a - h)$ at $h = 0.475$ and $(i - p)$ at $h = 0.625$.

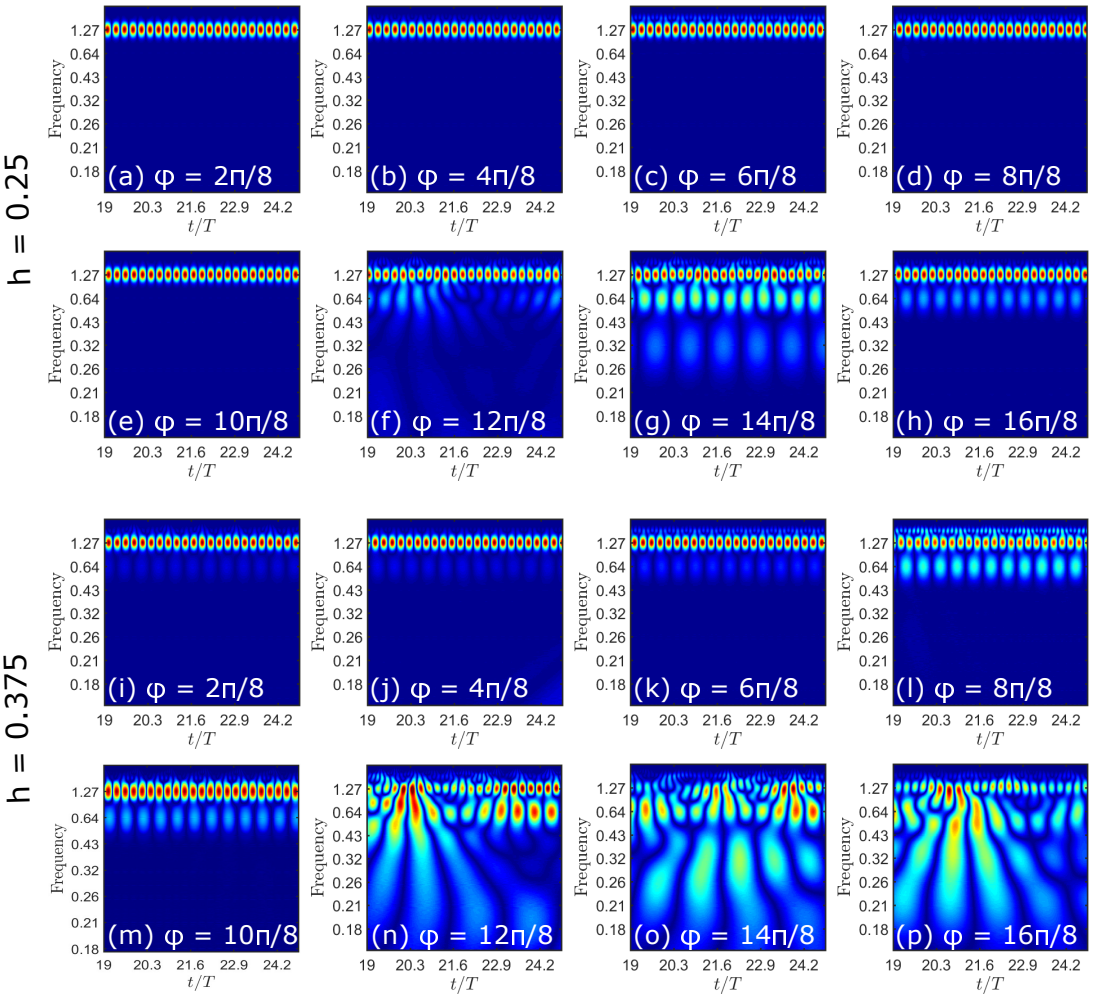

FIGURE 3. Morlet wavelet transform of the C_D time history at different ϕ values; $(a - h)$ at $h = 0.25$ and $(i - p)$ at $h = 0.375$.

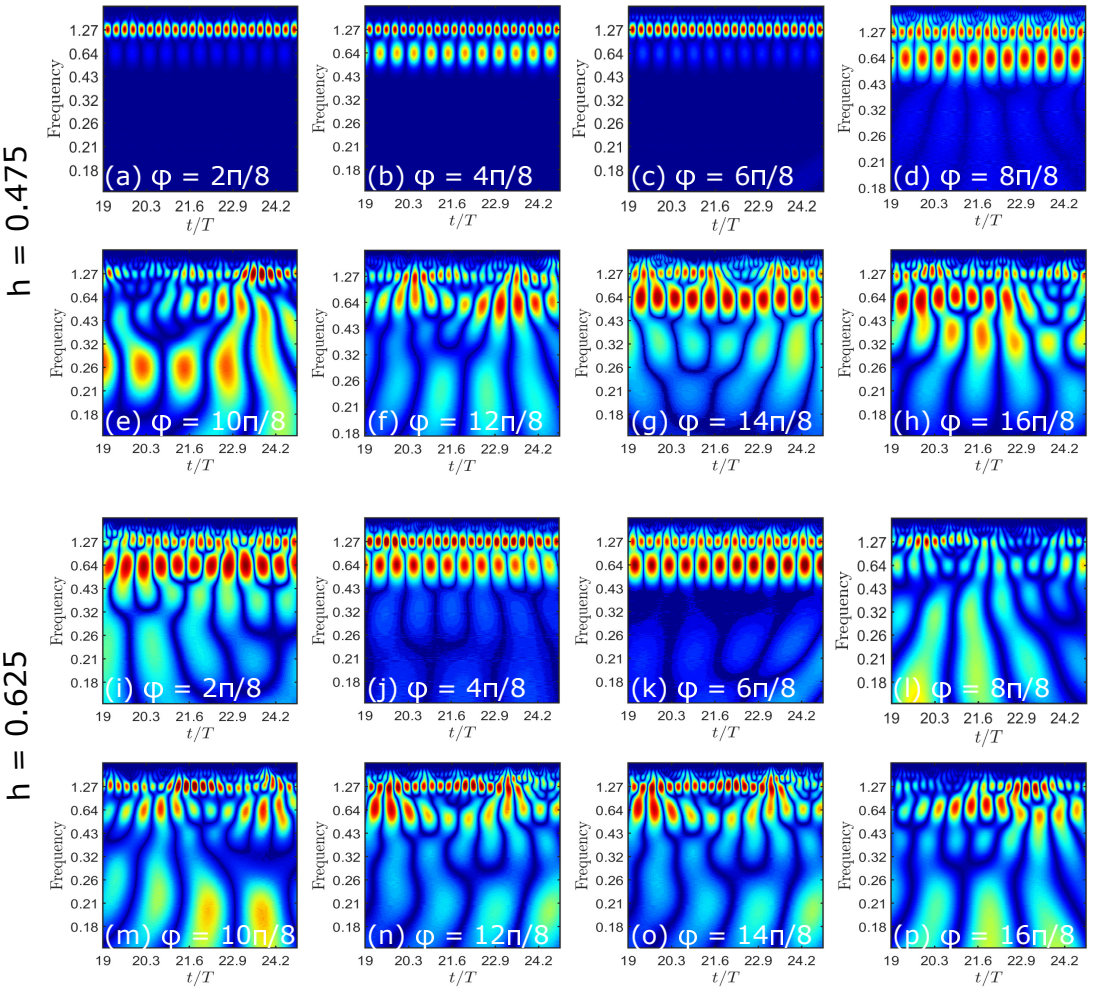

FIGURE 4. Morlet wavelet transform of the C_D time history at different ϕ values; $(a - h)$ at $h = 0.475$ and $(i - p)$ at $h = 0.625$.

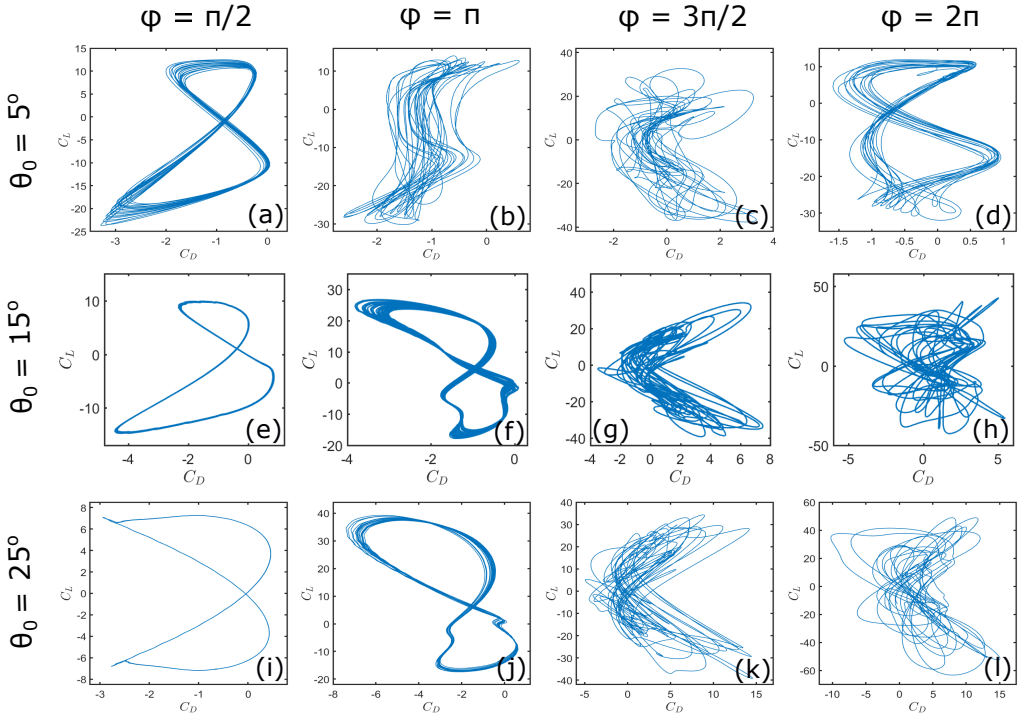

FIGURE 5. $C_L - C_D$ phase portraits for different pitch amplitudes and phase-offsets at $h = 0.475$, $\kappa = 4.0$, $x_0 = 0.5$ and $t_h/c = 0.12$.

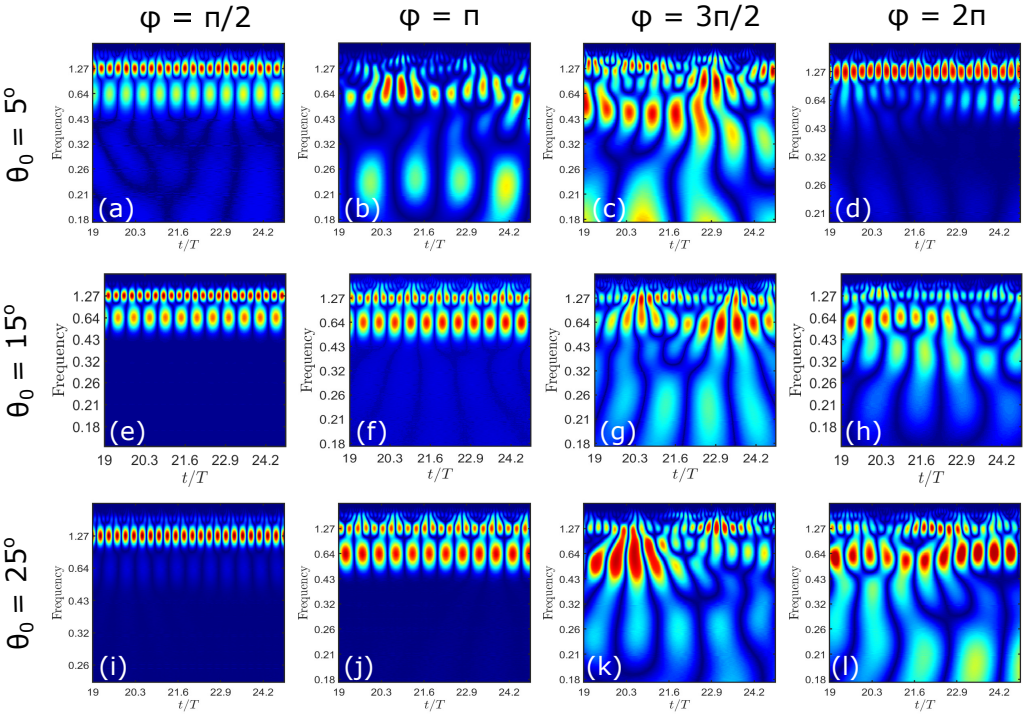

FIGURE 6. Morlet wavelet transform of the C_D time history for different pitch amplitudes and phase-offsets at $h = 0.475$, $\kappa = 4.0$, $x_0 = 0.5$ and $t_h/c = 0.12$.

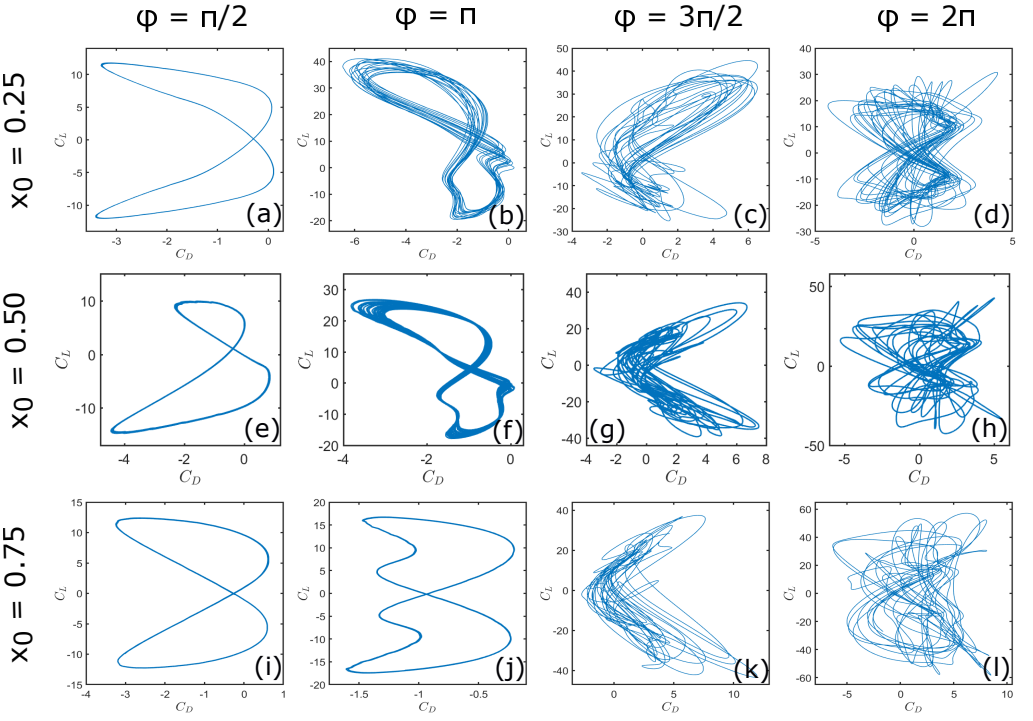

FIGURE 7. $C_L - C_D$ phase portraits for different pitching-axis locations and phase-offsets at $h = 0.475$, $\theta_0 = 15°$, $\kappa = 4.0$ and $t_h/c = 0.12$.

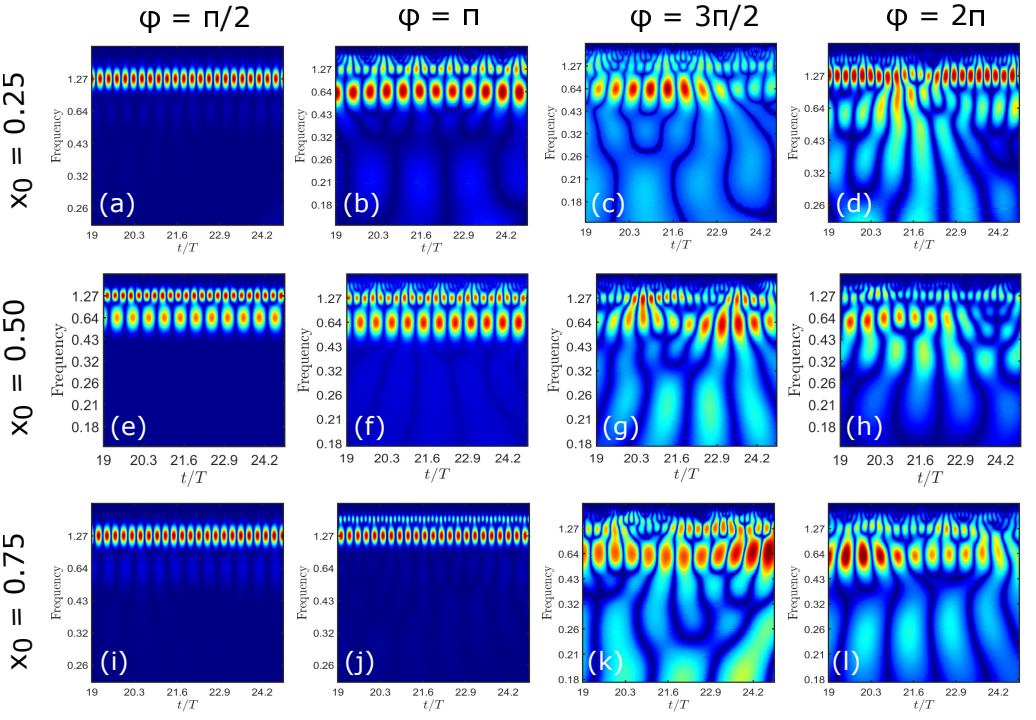

FIGURE 8. Morlet wavelet transform of the C_D time history for different pitching-axis locations and phase-offsets at $h = 0.475$, $\theta_0 = 15°$, $\kappa = 4.0$ and $t_h/c = 0.12$.

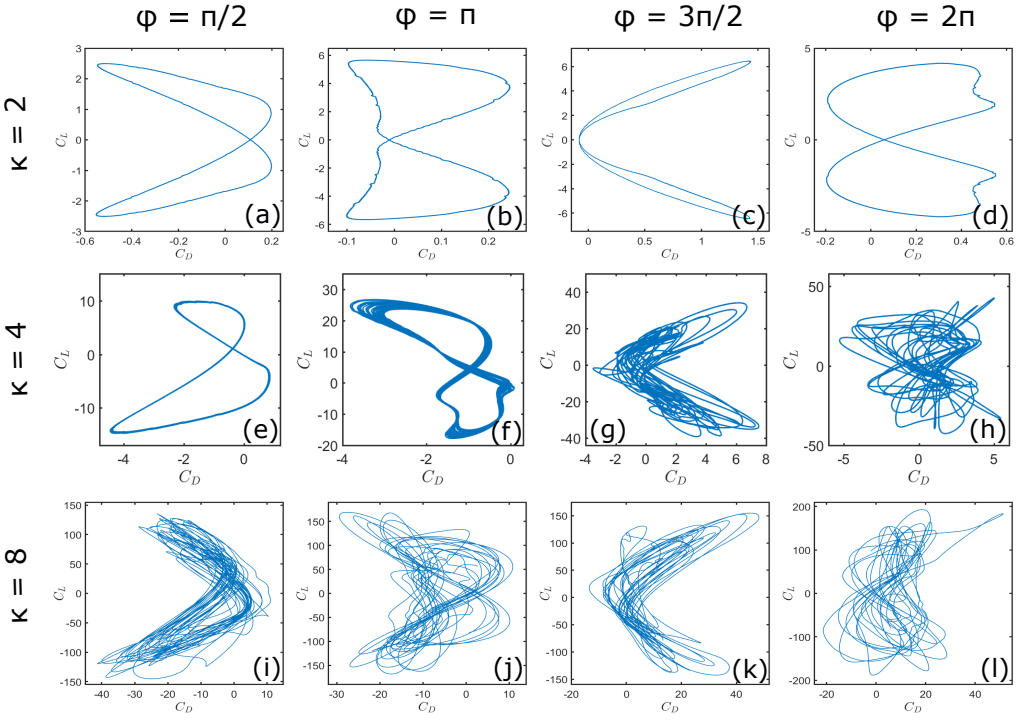

FIGURE 9. $C_L - C_D$ phase portraits for different flapping frequencies and phase-offsets at $h = 0.475$, $\theta_0 = 15°$, $x_0 = 0.5$ and $t_h/c = 0.12$.

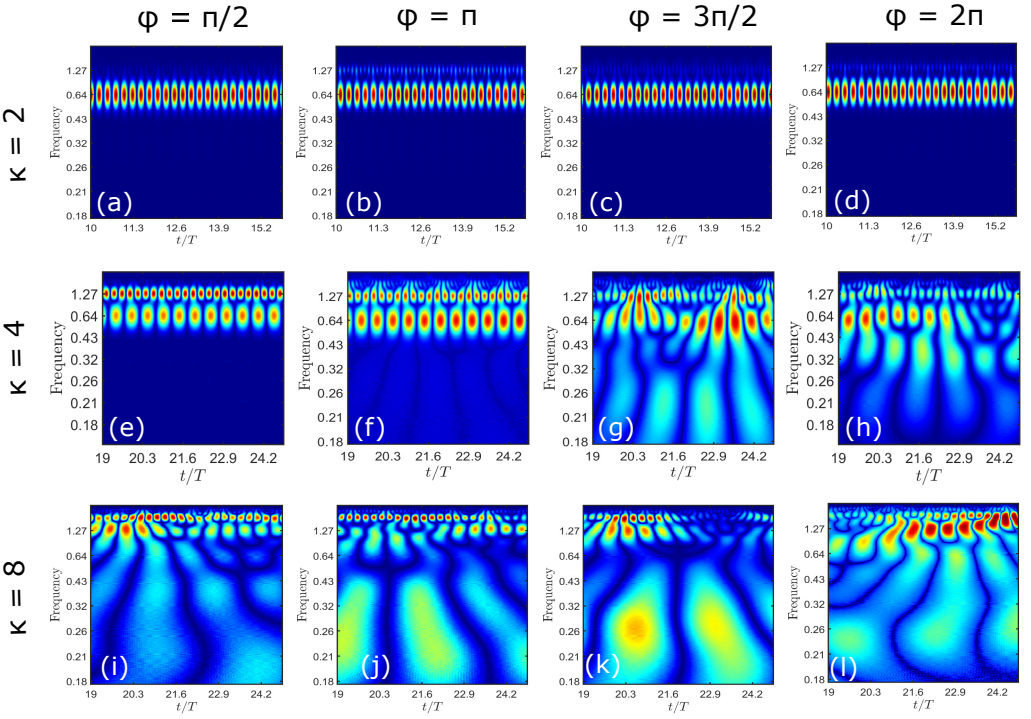

FIGURE 10. Morlet wavelet transform of the C_D time history for different flapping frequencies and phase-offsets at $h = 0.475$, $\theta_0 = 15°$, $x_0 = 0.5$ and $t_h/c = 0.12$.

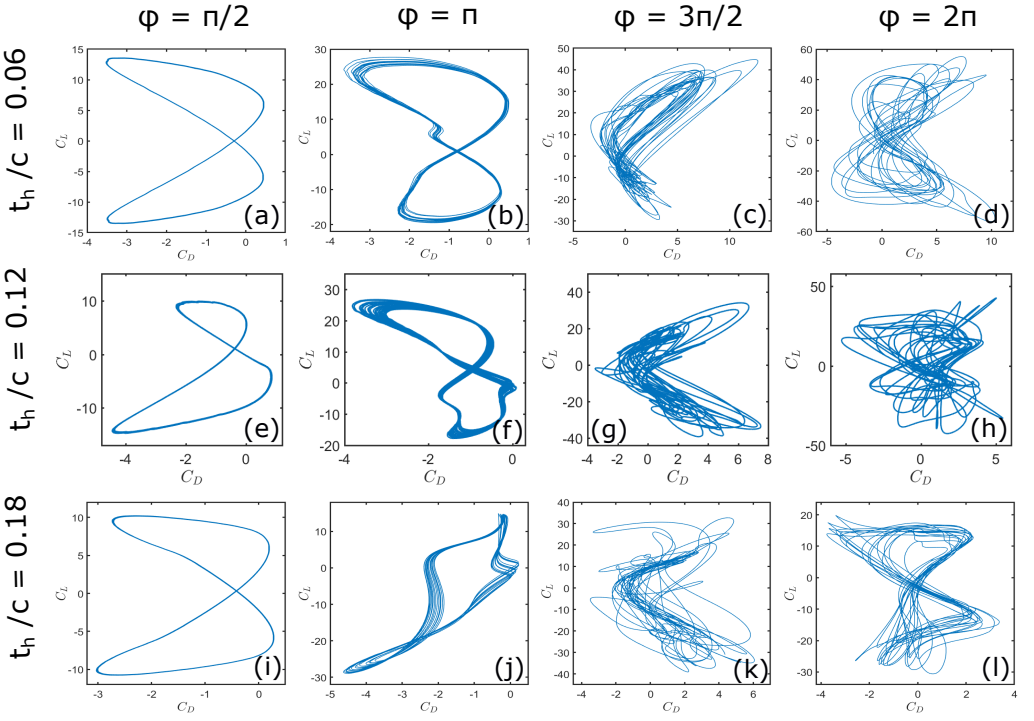

FIGURE 11. $C_L - C_D$ phase portraits for different foil thicknesses and phase-offsets at $h = 0.475$, $\theta_0 = 15°$, $\kappa = 4.0$ and $x_0 = 0.5$.

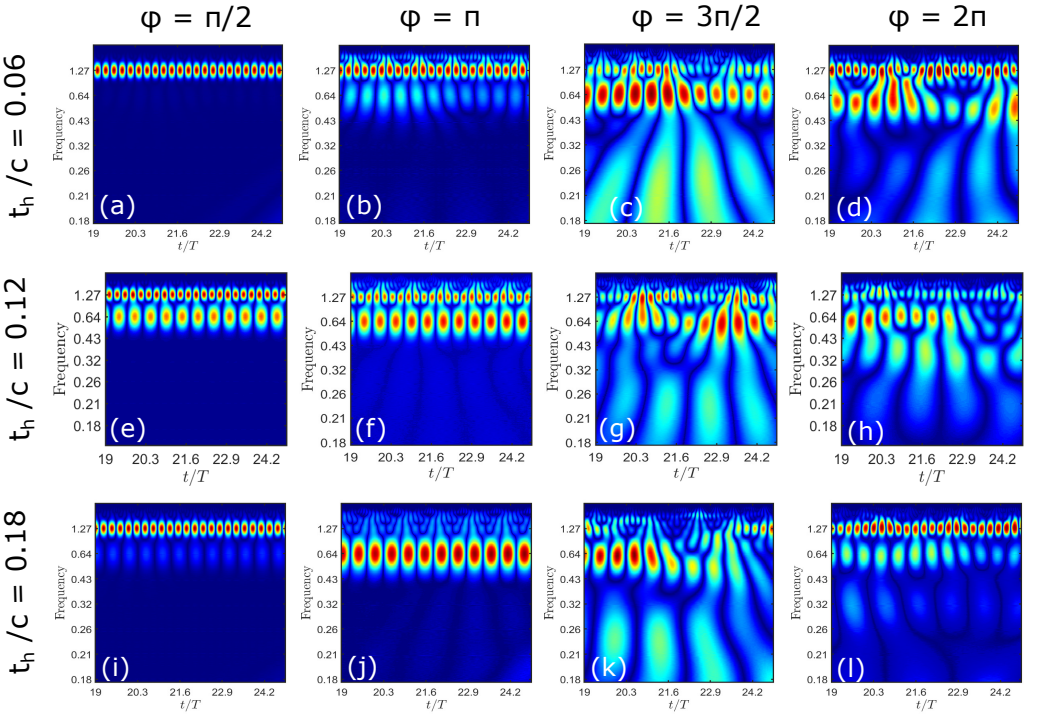

FIGURE 12. Morlet wavelet transform of the C_D time history for different foil thicknesses and phase-offsets at $h = 0.475$, $\theta_0 = 15°$, $\kappa = 4.0$ and $x_0 = 0.5$.

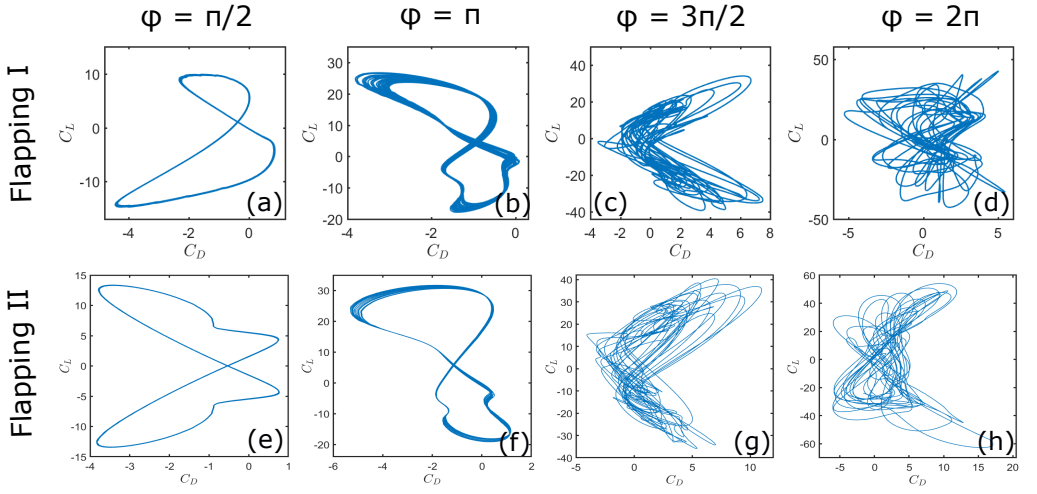

FIGURE 13. $C_L - C_D$ phase portraits for different flapping patterns and phase-offsets at $h = 0.475$, $\theta_0 = 15°$, $\kappa = 4.0$, $x_0 = 0.5$ and $t_h/c = 0.12$. Flapping I : sinusoidal plunge and sinusoidal pitch, Flapping II : sinusoidal plunge and trapezoidal pitch, and Flapping III : 'saw-toothed' pattern plunge and sinusoidal pitch.

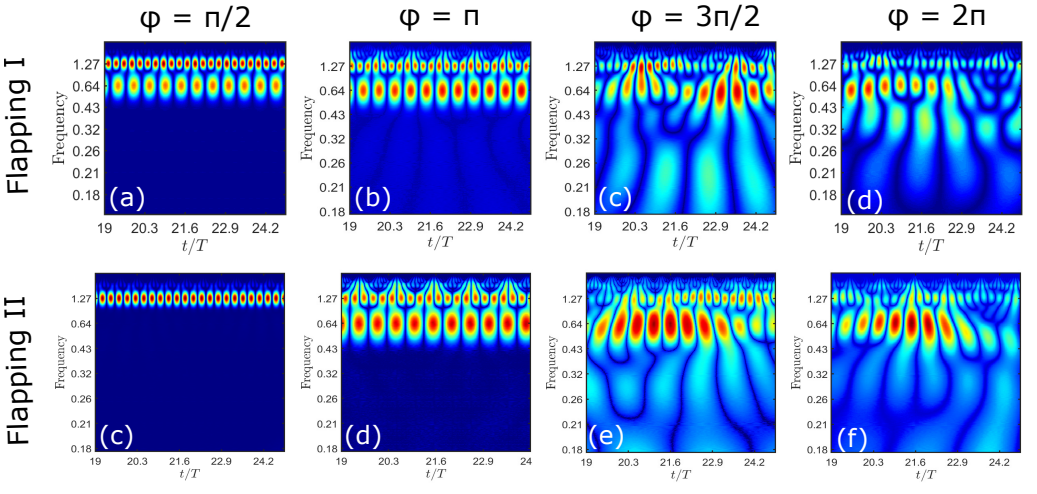

FIGURE 14. Morlet wavelet transform of the C_D time history for different flapping patterns and phase-offsets at $h = 0.475$, $\theta_0 = 15°$, $\kappa = 4.0$, $x_0 = 0.5$ and $t_h/c = 0.12$. Flapping I : sinusoidal plunge and sinusoidal pitch, Flapping II : sinusoidal plunge and trapezoidal pitch, and Flapping III : 'saw-toothed' pattern plunge and sinusoidal pitch.